Improved fine-scale transport model performance using AUV and HSI feedback in a tidally dominated system

L. F. Hibler and A. R. Maxwell
Pacific Northwest National Laboratory,
Sequim, Washington, USA

L. M. Miller
Max Planck Institute for Biogeochemistry,
Jena, Germany
Formerly at Pacific Northwest National Laboratory, Sequim,
Washington, USA

N. P. Kohn and D. L. Woodruff
Pacific Northwest National Laboratory,
Sequim, Washington, USA

M. J. Montes and J. H. Bowles
Naval Research Laboratory,
Washington, D. C., USA

M. A. Moline
Center for Coastal Marine Science, California Polytechnic State University,
San Luis Obispo, California, USA

Abstract

One of the challenges for model prediction and validation is providing them with data of appropriate spatial and temporal resolution. The maturation and increased application of autonomous underwater vehicles (AUVs) in aquatic environments allows systematic data collection on these model-relevant scales. The goal of this study was to apply a fine-scale circulation and transport model (Delft3D) to improve AUV mission planning and use data collected by the AUV to evaluate and improve model performance. A dye release was conducted in a tidally dominated embayment, and a planning phase model based on the best available data was used as a baseline for evaluation and for AUV mission planning (forecast). The planning phase model correctly predicted the general shape and direction of the dye plume and allowed for successful mission planning. Subsequently, bathymetry data collected by the AUV was incorporated into the model (hindcast), with temperature and salinity collected before the experiment. Comparisons with fluorometer measurements from the AUV indicate that the model effectively predicted the edges of the plume and centerline location. The location was also confirmed by remote sensing from an aircraft. Thermal stratification was found to be an important fate mechanism in the final model, and the results demonstrate the integration of observational data sets for small, short-duration surface-contaminant releases. This study highlights the strength of a phased, iterative approach with observation platforms and may serve as a guide toward improving the performance and evaluation of future coastal hydrodynamic and transport modeling efforts.

Keywords: plume model, autonomous underwater vehicle, hyperspectral imagery.

1. Introduction

Numerical models of circulation and associated fate and transport are used to gain an understanding of the (re)distribution of scalars such as heat, salt, nutrients, sediment, and anthropogenically derived materials due to planned and unplanned releases [e.g., Anwar, 1998; Stacey et al., 2000; Fong and Stacey, 2004; Grant et al., 2005]. Model projections support environmental impact assessment and can be used to assist in the development of sampling plans or monitoring programs, evaluation of remedial actions, and interpretation of observational data from a variety of sources [Arhonditsis and Brett, 2004; Lin et al., 2007; Liu et al., 2007]. As the numerical model complexity increases, for example, in moving to a three-dimensional as opposed to a two-dimensional application, and it is desired to resolve finer-scale hydrography or fate and transport processes, the challenges increase in terms of obtaining relevant observational data sets against which the model can be evaluated. Furthermore, for applied modeling studies, the desire to resolve the processes need to be balanced with computational feasibility.

Numerous field experiments have used rhodamine WT dye (RWT) to study dispersion in coastal settings. Stacey et al. [2000] used RWT to study dispersion off San Clemente Island, California resulting from a near-bed release and subsequent distribution below the thermocline. The data set of dye concentrations was used to adjust mixing coefficients for both a Lagrangian and Eulerian plume model and to assess each modeling methodology's utility in estimating scalar transport estimates and overall characterization of the resulting plume. Stacey et al. [2000] found that their Eulerian model overpredicted lateral dispersion and consequently underpredicted peak concentrations, but was able to correctly estimate the mean path of the dye plume. They demonstrated that a mixed analytic and numerical modeling coupled with ADCP surveys, and fluorometer arrays can be an effective approach for assessing scalar transport in open coastal environments. Fong and Stacey [2004] used RWT to study dispersion in the coastal water near Duck, NC. The focus of their study was the dispersion of material released near the bed and the formation of mixing coefficients based on empirical data and power law relationships for near-field and far-field cases. In contrast to the field program of Stacey et al. [2000], an autonomous underwater vehicles (AUV) (REMUS) sampled water for RWT concentrations. Similar to the findings reported by Stacey et al. [2000], the RWT transport upward was limited by the stratified conditions present at the time of the experiment. Both Stacey et al. [2000] and Fong and Stacey [2004] studies established mixing coefficients based on theory, flow velocities, and RWT observational data sets.

Anwar [1998] examined the horizontal and vertical mixing of two tracers (bromide-82 and gold-198) each introduced at different locations along the coast of the United Kingdom. The near surface releases were of sufficient duration to establish a plume which was considered developed and steady for the temporal and

spatial scales of interest (a few hours and about 10 km). Unstratified and stratified cases were examined. Radioactivity levels were obtained with surface vessel surveys; these were decay corrected and longitudinal, lateral and vertical mixing relationships were fit to this data. Vertical and lateral tracer distributions were found to be Gaussian when currents were spatially uniform. The tracer spreading rate was found to fit a nonlinear function in stratified waters. Vertical spreading in stratified conditions was limited to the location of the pycnocline and above. On multiple lateral passes through the plume closely spaced in time, the location of maximum concentration shifted randomly indicating the presence of eddies within the mean flow. Similar studies were reported by Ledwell et al. [2004], Houghton [2002], and Stacey et al. [2000].

In consideration of these factors, this modeling study was designed to resolve the dominant features of transport of a short-duration release of dye at a spatial scale that would be representative of realistically constrained applied coastal modeling efforts. The specific aim was to demonstrate that a three-dimensional coastal circulation and transport model coupled with AUV and remote imagery can be an effective approach for understanding scalar advection and mixing resulting from a surface release in a complex, tidally dominated, thermally stratified environment. To address this, a short-duration plume of RWT was released into Sequim Bay, WA and a field program was designed to document its transport where wind generated waves are insignificant. A planning model was used to guide the field experiment, and the in situ data and hyperspectral imagery (HSI) collected during the experiment were used to evaluate the model performance and guide its improvement during the intermediate and final modeling phases. The present study differs from others in terms of the dimensionality of the model used, the scale of the release, and a surface rather than a bottom release [Ramos et al., 2006].

2. Model and Experimental Approach

2.1. Site Description

--- Insert Figure 1 ---

Sequim Bay is a small (≈2.5 × 8 km) embayment, connected to the Strait of Juan de Fuca (Figure 1). The narrow mouth of the bay (150 m), relatively large area (19.7 km^2) and moderate tidal range contribute to a strong, dynamic, and spatially complex circulation in the northern portion of the bay, with features including eddies and tidal fronts [Marmorino and Smith, 2007].

The circulation of Sequim Bay has not been reported in detail, and little observational data is available except in a recent study by Marmorino and Smith [2007]. Conceptually, the bay is thought to have two cells (north and south) [Elwha-Dungeness Planning Unit, 2005]. The northern half is thought to be stratified, and includes Middle Ground, a shoal near the bay mouth which divides tidal flows. The southern half is thought to have a single layer, and the transition between the two-layer and single-layer areas is the working delineation of the north and south portions of the bay, though the location is not reported. The southern cell is poorly flushed and exhibits a weak counterclockwise (cyclonic) circulation [Elwha-Dungeness Planning Unit, 2005]. This characterization is consistent with the infrared imagery analysis reported by Marmorino and Smith [2007]. The typical salinity within Sequim Bay ranges from 30 (during spring) to 32.5 (late summer). This is largely consistent with water outside of the bay. During storms and spring runoff some freshing of the bay does occur, causing a halocline to develop. The temperature of Sequim Bay water is about 8°C in winter and up to 16°C in the summer [Brown and Caldwell Consultants, 1992]. Surface heating and light winds in the summer can lead to thermal stratification which is most likely to be more pronounced at the head of the bay. Given the shallowness of the southern bay, moderate winds can effectively destratify the water column. The maximum depth within Sequim Bay is 40 m, and depths near the head of the bay are less than 10 m. Thermal variations in the northern portion of the bay are most attributable to the inflow of water from the Strait of Juan de Fuca as is shown by infrared imagery by Marmorino and Smith [2007].

Foreman et al. [1995] developed a barotropic tidal model including portions of the Straits of Juan de Fuca and Georgia. Their study area included the outer portion of the model domain used in this study, but Sequim Bay itself was unresolved. The calibrated model of Foreman et al. [1995] included eight tidal harmonics (M2, S2, N2, K1, O1, P1, and Q1). They conducted a harmonic analysis on the estimated model and observed tidal records, and produced cotidal charts for the M2 and K1 harmonics. Just outside the mouth of Sequim Bay, the M2 and K1 amplitudes were estimated to be 55 cm and 69 cm, respectively, with corresponding phase estimates of 329° and 65°. They reported that S2, N2, and K2 results were correlated to the M2 results with amplitudes being 28%, 20%, and 7% of the M2 amplitudes, and phases greater than the M2 by 25°, −30°, and 25°. Similarly the O1, P1, and Q1 were correlated to the K1 results with amplitudes being 55%, 31%, and 11% of the K1 amplitude and phases less than the K1 by 29°, 3°, and 30°. Given these estimates, the tidal form factor $F = (K1 + O1)/(M2 + S2)$ is 1.51. Tidal form factors in this range are in the borderline class of mixed, mainly diurnal.

Tidal elevations in Sequim Bay range from −1.37 m to 3.51 m relative to mean lower low water (MLLW), and the tidal exchange between the Strait of Juan de Fuca and Sequim Bay is much larger than any freshwater discharge into the bay [Brown and Caldwell Consultants, 1992; Elwha-Dungeness

Planning Unit, 2005]. The spring tidal range for Port Townsend, WA and Victoria, Canada are 1.8 m and 1.0 m, respectively [Mofjeld and Larsen, 1984]. Both of these sites are on the Strait of Juan de Fuca and are microtidal to nearly mesotidal range.

Tidally driven water enters Sequim Bay through its narrow (≈150 m) mouth on flood tide. Near the dye release site, the flow is divided into a portion that flows alongshore on the west side of Middle Ground and the remaining toward the center of the bay to the east of Middle Ground. Middle Ground is an emergent shoal only during the low tide, with an elevation of 0.6 m above MLLW. As the tide rises, Middle Ground becomes more submerged and consequently presents less of an impediment to flow going toward the south. During this tidal phase, water that enters Sequim Bay is not diverted toward the east but joins the dominant southward flow along the west boundary of the bay. To the authors' knowledge there are no analyses of tidal currents within Sequim Bay against which to evaluate the model developed in the present study.

2.2. Model

2.2.1. Basic Description

A three-dimensional circulation and transport model was developed for Sequim Bay and a portion of the Strait of Juan de Fuca using WL|Delft Delft3D-FLOW software (hereafter referred to as Delft3D). A fine mesh was nested within a larger, coarser computational mesh (Figure 1), and RWT was treated as a conservative tracer within the modeling framework. The data used to initialize the numerical model and evaluate model performance are discussed in subsequent sections.

Tidal, wind-driven and density-driven circulation were accounted for in the model. The effects of bathymetry, Earth's rotation and bed stress are also included. The general model analysis was configured with the assumption that there was limited effect of nonhydrostatics, surface heating and cooling, RWT decay, movement of the RWT release source, and unsteady delivery of RWT mass over the release period. The model is based on the continuity equation and horizontal momentum equation and uses a turbulence closure submodel to adjust mixing rates as a function of flow conditions. The model domain is represented by a orthogonal curvilinear mesh in the horizontal and a terrain following (σ-) coordinate system in the vertical. The model numerics are fully documented by WL Delft Hydraulics [2003], and it has been used to conduct various modeling studies [e.g., Hesselink et al., 2003; Bielecka and Kazmierski, 2003].

A three phase (planning, intermediate, and final) model application approach was employed. The important differences between these phases are shown in Table 1. In general, field data (bathymetry,

temperature, salinity) was incorporated into the model as it became available, and model parameters were altered in order to more closely correspond with measured plume behavior. In the intermediate and final models the finer resolution mesh was extended to the south.

--- Insert Table 1 ---

2.2.2. Planning Phase Simulation

The model mesh was developed on the basis of the best bathymetry information available that provided comprehensive coverage within the bay and the area of the Strait of Juan de Fuca just outside Sequim Bay (Figure 1). This was a publicly available gridded 10 m resolution data set [Finlayson, 2005], which was transformed to a Cartesian coordinate system (UTM Zone 10N, WGS84). The shoreline evident at the spatial scale of this data set was used to represent the closed boundary of the model. It was assumed that the available bathymetry data was sufficient to produce an initial plume trajectory estimate.

A model mesh was extended to distant open boundaries so that circulation near the area of interest (the Sequim Bay mouth) was driven by model physics rather than the artificiality introduced by proximity to these boundaries. The tidal elevation conditions along all open boundaries were set to available tidal predictions from Xtide (D. Flater, XTide version 2.8.2, harmonics-dwf-2006-07-08, http://www.flaterco.com/xtide, 2006) for Whidbey Island (on the northeast corner of the model domain), Dungeness Spit (on the west boundary) and Port Townsend (on the east boundary) so that the model could be run in a predictive mode. The tidal boundary time series from (D. Flater, http://www.flaterco.com/xtide, 2006) was linearly interpolated between corners of the model domain. The tidal predictions used to drive the model are consistent with the study of Foreman et al. [1995], although the simulations were not of sufficient duration to conduct a formal harmonic analysis. In the present study, it was assumed that the actual future tidal conditions were reasonably represented with XTide predictions.

In this phase of model application, no surface winds were applied because forecasts were lacking and light winds are typical in Sequim Bay during the summer. It was further assumed that it was practical to treat the water column as completely mixed because of the lack of observational data to specify otherwise.

This mesh had 108 × 132 horizontal computation cells, and the water column was subdivided into ten layers. A finer resolution mesh (187 × 145 horizontal cells) was nested within the coarse mesh in order to

focus on the region near the RWT release location. A free-slip sidewall boundary was applied. While the number of vertical layers remained the same for both meshes, the vertical resolution differed (Table 3). The circulation within the finer resolution model was driven by tidal elevations provided by the coarse model results, archived every 5 min over the period of interest. A summary of these model mesh parameters is given in Tables 2 and 3, and the meshes are shown in Figure 1.

2.3. Field Experiment

2.3.1. ADCP and CTD

---Insert Figure 2 ---

For several weeks prior to and during the dye release on 24 July 2006, an upward looking 1200 kHz RD Instruments acoustic Doppler current profiler (ADCP) was deployed at the bottom of the Sequim Bay entrance channel to document the current regime over at least one spring tidal cycle. The channel depth at this point is about 8 m at MLLW. ADCP data were binned into 40 25-cm vertical layers; these data were filtered and reported every 8.7 seconds. A Seabird SBE19 profiling CTD was used to collect CTD profiles at the start of the ebb tide, and low tide and at flood tide at four locations near the outer and inner corners of the nested model domain shown in Figure 1. However, there was not sufficient time to incorporate this information into the model for the planning phase of the dye release effort. The lack of stratification data for model initialization was not expected to be a significant problem, as the circulation predicted by the model agreed qualitatively with observations, and the plume was expected to be primarily driven by advective forces. Final simulations were performed using the CTD profile shown in Figure 2, and will be discussed later in this paper. The CTD profiles did not differ significantly in the location of the upper layer with respect to the locations sampled.

2.3.2. Dye Plume

--- Insert Table 2 ---

--- Insert Table 3 ---

--- Insert Figure 3 ---

A small surface discharge was created using RWT. RWT was selected for its prior use as a conservative tracer in marine water [Stacey et al., 2000; Fong and Stacey, 2004; Ledwell et al., 2004], and because its fluorescent activity is not subject to interference by particles, is not photodegraded or biodegraded in the timescale of interest (less than 1 day), and because it can be detected and measured by in situ and remote sensing techniques. This release was conducted during a daytime flood tide from a vessel anchored inside the mouth of Sequim Bay (Figures 1 and 3) , where rapid RWT dilution and dispersion was expected. Because one of the objectives of the RWT studies was to evaluate detection of water properties by remote means, the surface release created a high-contrast RWT surface area larger than several hyperspectral image (HSI) pixels so that a maximum RWT signal (and potentially intermediate RWT signals) could be spectrally differentiated from surrounding water. A flux rate of 9.9 g/min RWT was maintained by using a fluid metering pump to feed the RWT into seawater as it was passed 2.4 m through a pipe to its release point. The average seawater flow rate was 16.7 L/min, and complete mixing was assumed to occur over the length of this pipe. The release point was approximately 0.2 m below the water surface. RWT was released for 77 min (1533 to 1650 Pacific daylight time) for a total release of 762 g RWT. The dye was not premixed with fresh water or other solvent as it was determined that the dye would be sufficiently mixed with seawater and its density at the release point would be within 0.001 kg/m^3 of the receiving water. The average release concentration of RWT was determined to be 6×10^5 μg/L (ppb), based on measurement of ten samples collected from the release pipe (7% CV).

In coastal waters, RWT is visible to the human eye down to concentrations of about 50 μg/L and the fluorometer onboard the AUV has RWT detection limit of about 1 μg/L. On the basis of these criteria, the maximum observable dilution of RWT under these conditions ranges from 1:10,000 to 1:1,000,000. The HSI RWT detection limit has not been established for Sequim Bay water conditions.

2.3.3. REMUS Description

In order to detect and map the RWT dye plume in this experiment, a Wetlabs Inc. ECO-Triplet (chlorophyll, backscatter and rhodamine) fluorometer was integrated into a REMUS AUV platform [Moline et al., 2005b]. The REMUS-100 vehicle used in this study is a propeller-driven platform that navigates by compass or relative to seafloor transponders via Long-Baseline (LBL) and/or Ultra Short Baseline (USBL) acoustics located throughout a network area, allowing for multiple flight path options

within the defined volume space. The vehicle also incorporates a GPS system for improving navigation or exclusively for missions without acoustic navigation. Four lithium batteries supply 1 kW of power to the REMUS allowing missions of 6–8 h at a nominal speed of 1.6 m/s. The electrical integration of the module to the REMUS vehicle includes power, serial connections to the sensors, providing data and a debug capability through the REMUS GUI, and leak detection for mission planning and abort sequences. Aft of the sensor module is an Ocean Sensors OS-200 CTD that, in addition to oceanographic measurements, is used for speed of sound estimates and vehicle depth. A 1200 kHz RDI-ACDP provides estimates of currents 20 m above and below the vehicle, altimetry for mission planning, and Doppler velocimeter logging for navigation [Fong and Jones, 2006]. The combination of the altimetry with the vehicle depth provided the bathymetry data used in this study. The vehicle is preprogrammed on the basis of general knowledge of the area. The small size allows for easy transportation, and may be launched and recovered from a small vessel or pier without special handling equipment. Data is downloaded via an Ethernet connection on recovery of the vehicle.

2.3.4. REMUS Mission Planning

Using the predicted streamlines from the preliminary model, the AUV was programmed to fly a 400 × 100 m (nominal) grid consisting of 40 transects spaced 10 meters apart (Figure 3). The vehicle depth was set to 1 m during the mission to help ensure sensing of the surface plume. As Middle Ground was near or at the depth of operation, there was a 2 m water depth threshold at which the vehicle would turn around and continue to the following waypoint. Navigation during the mission was by acoustic triangulation based on LBL communications with three transponders placed ≈1.5 km from the study grid. The total distance of the mission was 4.5 km with a programmed velocity of 1.6 m/s. Additional details on general mission planning for the REMUS-100 are provided by Moline et al. [2007].

2.3.5. PHILLS Description

Hyperspectral images were acquired using the Naval Research Laboratory's aircraft-mounted Portable Hyperspectral Imager for Low-Light Spectroscopy (PHILLS). On 24 July 2006, 41 PHILLS images were collected in alternating northeast and southwest flight paths. Aircraft altitude varied between 1,000 and 3,000 m, resulting in a 0.5–1.5 m pixel size over wavelengths of 400–1,000 nm. The PHILLS sensor is linked to an inertial measurement unit to record the pitch and roll of the airborne platform as well as a kinematic GPS for recording precise location and elevation information [Davis et al., 1999, 2002]. The data from these sensor systems are used to create a geographic lookup table file that is used to precisely reference the images.

3. Results and Discussion

3.1. Planning Simulation

3.1.1. General Features

Delft3D simulations were conducted with repeated tidal forcing to investigate the bay circulation. On ebb tide, flow is predicted to converge over Middle Ground, while on flood, tidal flow is predicted to separate around Middle Ground. A small eddy forms at the head of Travis Spit on ebb tide, while on flood tide, small eddies are estimated to form on the southern shore of Travis Spit and on the northern western edge of the Sequim Bay entrance channel. These modeled features are qualitatively consistent with visual observations, but observational data sets to quantitatively assess the model are not available.

3.1.2. Plume Prediction

--- Insert Figure 4 ---

--- Insert Figure 5 ---

Planning phase model results for plume track prediction are shown as a dotted contour, labeled "Planning" in Figure 4. This model correctly predicts that the overall direction of the plume is south–southwest, but ultimately fails in predicting the shape. Streamlines visualized in the 3D velocity field with DataTank (see http://www.visualdatatools.com/) indicated that release point position would significantly influence the plume trajectory because of recirculation patterns along Middle Ground which lead to dead zones and flow reversals. These are shown in Figure 5.

3.2. Incorporating Measurements in Simulation

3.2.1. AUV

In defining the position of plume fronts and comparison with model output, it is important to quantify the uncertainties in the spatial position of the field observations. There are two sources of positional uncertainty in the rhodamine dye measurements made by the REMUS AUV. These include the sampling resolution of the rhodamine flurometer/AUV combination and the uncertainties in the LBL acoustic triangulation for navigation. Given the sampling rate of the rhodamine fluorometer (0.91 Hz) and the nominal speed of the vehicle for this study (1.60 ± 0.07 m/s), based on the time taken for each transect

line detecting rhodamine dye (n = 18), the distance between observations was 1.76 ± 0.08 m. The navigational uncertainty is a combination of the GPS uncertainty in the placement of the transponder locations and the distance from each of the transponders, which forms an ellipse of uncertainty around any given location. With an estimated uncertainty in the GPS location of 4 m, and distances from the plume to the transponders ranging from 783–1100 m, an uncertainty ellipse with primary and secondary axes of 9 and 8 m was found. The combined horizontal uncertainties were therefore on the order of 10 m, which is within the spatial resolution of the fine mesh (Table 2) used in this study. The mean operational depth of the vehicle during the mission was 0.84 ± 0.32 m. For comparison with model-predicted concentrations of rhodamine dye, the AUV-based observations at this depth range were compared to model values interpolated in three-dimensional space (cubic spline) and time (linear) to be as consistent as possible with these observations. Again, the model resolution was coarser than the observations, making direct comparison within the mesh space valid.

--- Insert Figure 6 ---

Comparison of the initial gridded bathymetry used, the AUV surveyed bathymetry, and the final composite of these, reveals significant variations in the data sets. Aside from the submodel spatial-scale variation in the bathymetry that is apparent in the AUV survey, it is clear that bathymetric features differ at the mesh spatial scale and above. The bathymetry variation between these data are shown in Figure 6 for transects that approximate the longitudinal and lateral axis of the RWT plume.

In Figure 6, the transect labeled “Planning” represents the DEM bathymetry [Finlayson, 2005]. Multiple AUV surveys were performed over a period of several days, accumulating measurements at each sample location (dotted track) shown in Figure 6a. Figure 6a also shows the dye release area as a darkened region, as more points were gathered in this area from overlapping surveys. The “REMUS” transect was produced by a simple merge of the DEM bathymetry with the AUV sampled bathymetry, using Delft3D-QUICKIN software. Some discrepancies were noted using this method, primarily because of outliers in the AUV data set where the vehicle came too close to the bottom. The “Final” transect was produced by a weighted averaging of the DEM surface with nearby survey points using DataTank, and weighting parameters were adjusted to interactively smooth out obvious outliers in the AUV bathymetry while viewing a 3D surface plot of the merged data set.

3.2.2. HSI

Six images were processed to reveal the RWT signal over time. Table 4 shows the processing details of a selection from this data set. The image processing entailed coregistering the processed images to a common geographic location, masking out the land pixels as well as those dominated by sun glint, and then forming the ratio of the reflectance specific bands. For geopositioning, Run 14 was used as the baseline. For relating in situ spectral information and atmospheric corrections, Run 29 provided the best comparison to HSI and so was used as the reference image. Within each image a common geographic feature on the northeast corner of Middle Ground is identifiable. Each image was realigned by translation to match this location with coordinates given for Run 14; rotation of the image was not considered because of limited ground fixes. The level of geographic adjustment (up to 35 meters) required is indicative of the geographic spatial uncertainty in this data set. During the course of the field experiment, the release vessel moved slightly (≈10 meters). From the modeling input perspective this release position was fixed to 48.07530N, 123.03740W in UTM Zone 10N WGS84.

--- Insert Table 4 ---

To correct for atmospheric light attenuation, the PHILLS images were adjusted to Analytical Spectral Device (ASD) spectra. The near surface ASD spectrum used for this analysis was taken at 1641 PDT at a Sequim Bay Station (48.07405N, 123.03764W) and nearly coincides with the time of Run 29. To compensate for inherent HSI spectra noise, all images were subset to 407.4–893.9 nm (51 bands of data). ASD input data was also subset to 401.07–889.82 nm. Spectral empirical line fit (ELF) window for application to Run 29 used a 5 × 5 pixel (≈2.5 × 2.5 m) sample window to alleviate Sun glint pixels; the location is southeast of Middle Ground so bottom should be of consistent depth in a 5 × 5 pixel window. Run 29 was then used to achieve a deep water spectra inside Sequim Bay at the following location: 48.07761N, 123.03561W (UTM 10N WGS84). In order to remove land and sun glint dominated pixels, the images were masked by thresholding the 806.0 nm band at remote sensing reflectance values below 0.009. In order to extract the RWT signal from PHILLS images, the band ratio was formed on the ELF fit for bands 592.2 nm and 533.6 nm. Most images had multiple pixels at the maximum band ratio for that image, which decreased over time as shown in Table 4.

3.3. Intermediate and Final Simulations

3.3.1. General Features

Following the field experiment, in situ measurements were used to reinitialize the simulations, with varying degrees of improvement. First, for the intermediate model simulation, high-resolution bathymetric data collected by the REMUS AUV was incorporated into the simulation. The simulated plume using the modified bathymetric data set is shown as a coarse dashed line in Figure 4, the longest contour in Figure 4. It is apparent that the bathymetric differences were significant in this case, at least for the size of the plume considered. However, the model advection was too strong in this scenario, and the direction trended strongly southward, which was inconsistent with PHILLS and the AUV observations. Changing the model wall boundary condition to no-slip instead of free-slip significantly altered the dye distribution at a low eddy diffusivity. However, at the eddy diffusivity shown here, the impact of the wall boundary condition variation was minimal. In this phase of the study, the accuracy of the model bathymetry was somewhat improved by incorporation of the AUV survey data. However, because the AUV survey did not cover the entire model domain, much of the original bathymetric data was still relied upon. The second and final modification was to incorporate more realistic stratification into the model, using CTD measurements taken before the dye release. A single point CTD profile taken near the northwest boundary corner was used to reinitialize the nested simulation, applied as a 3D spatially varied boundary condition. The planning (dotted), intermediate (dashed), final (solid) simulated plume outlines and the HSI-derived plume area are shown on Figure 4. This final addition of thermal stratification improved the prediction significantly. Both direction and length of the simulated plume were affected by this change.

Brunt-Väisälä (buoyancy) frequency (expressed in hertz), N, is a measure of the vertical stability of the water column [Pond and Pickard, 1983]:

$$N^2 \approx g\left(-\frac{1}{\rho}\frac{\partial \sigma_t}{\partial z}\right) \qquad (1)$$

where $\sigma_t = \rho\,(S, T, P = 0) - 1000$ expressed in kg/m^3, g is gravitational acceleration, z is vertical position (negative downward). The gradient Richardson number, Ri_g is the ratio of density to mechanical stability.

$$Ri_g = \frac{N^2}{(\partial u/\partial z)^2} \qquad (2)$$

Using the final simulation results, the minimum values of Ri_g were computed to be about 0.1, 1.0 and 4.0 within the mouth of Sequim Bay, at the RWT release location and the plume center for depths of 2 to 4 meters. In cases where Ri_g is less than 1/4, turbulent mixing in the vertical is enhanced either because of unstable (or weakly stable) density profiles or excessive horizontal shear. Not surprisingly, turbulence within the mouth of Sequim Bay would be expected to provide effective mixing and this tendency is expected to diminish toward the interior of the bay. Turbulent vertical mixing is not expected to significantly transport dye below the upper portion of the water column within the interior of the bay over the distances and times that were examined in this study.

3.3.2. ADCP

--- Insert Figure 7 ---

--- Insert Figure 8 ---

--- Insert Figure 9 ---

Figure 7 shows the comparison of the final model output to the ADCP data. During the flood tide, the model does not achieve current magnitudes as high as those measured by the ADCP. Between high high and high low tide, the model currents are larger for longer periods than the ADCP record shows. As the tide ebbs to low low, better agreement in current magnitude and phase is achieved. Figures 8 and 9 show the measured and predicted velocity at the 4 m elevation as a time series and scatterplot, respectively. A box filter with a window of 4 min was applied to the ADCP data in Figures 8 and 9 in order to demonstrate trends in the ADCP measurements on the timescale of the model output. This removes some of the high-frequency variation shown in Figure 7.

3.3.3. Comparison With HSI

The 592.2/533.6 nm ratios were considered as normalized RWT signal strength. It is not clear over what depth the reflectance represents. In order to more qualitatively compare these RWT signals or model results or AUV fluorimeter data, an assumption would need to be made regarding the vertical distribution

of the HSI-derived signal strengths. On the basis of the estimated Ri_g values, the majority of the RWT signal would be derived from the upper few meters of the water column. A normalized contour from two of these processed images is shown in Figure 4.

3.3.4. Comparison With REMUS

--- Insert Figure 10 ---

The AUV tracks are shown in Figure 3, and the fluorometer recordings are shown in Figure 10a. The model results are interpolated in 3D space and time in order to compare with the AUV fluorimeter data. Interpolated Delft3D estimates were positioned at the AUV location relative to the water surface rather than the height above bottom. This comparison is also shown in Figure 10a.

--- Insert Figure 11 ---

The RWT concentrations measured during the REMUS deployment were divided into 18 2-min long passes through the RWT plume. Delft3D model projections were interpolated in time and space for the purpose of comparing the two. Observed and estimated RWT concentrations for each pass are shown in the multipanel Figure 10. The peak value within each pass is shown for both the AUV observation and Delft3D estimate. The time recorded for each peak within a pass for both these data sets are plotted against each other in Figure 11. Delft3D results are plotted for two cases (differing by inclusion of density stratification and free-slip boundary conditions).

The deviations between observed and estimated peak concentration within each pass are significant but are well within an order of magnitude; the largest deviations is found in pass #14. As expected the observation data show more variability than the estimated RWT concentrations. The observed plume is shown to be narrower and more peaked than the model estimate. The time-at-peak intercomparison (Figure 11) shows a high correlation between the observations and model estimate. This shows that the model performs very well during the moderate dilution phase at estimation of the time-space location of the plume centerline while not capturing peak concentrations as well. This finding is consistent with that reported by Stacey et al. [2000], and understandable given the nature of the Eulerian model.

4. Conclusions

4.1. Summary

This modeling effort has provided the first physically based quantification of the complex flows around the mouth of Sequim Bay that account for Middle Ground, an intertidal shoal. The presence of this shoal provides a significant control on the division of flow in the northern portion of bay. The complex circulation in this portion of the bay was found to greatly influence the RWT transport.

Model currents compare well to the ADCP data within the mouth of Sequim Bay. The model does not reproduce the high-frequency oscillations in flow found by the ADCP. However, the tidal velocities match well, on average, in terms of matching timing and amplitude of current peaks. Analysis of the HSI plume delineations indicates that there are finer-scale features evident in the plume that the model has not resolved. This is due to a variety of causes. The model resolution is O(10 m) and the discernible features have scales as small as a few meters. Bathymetry details and the shore line are at sub-grid scales, and features outside of the surveyed area are likely influencing plume behavior. Although measured winds are applied to the intermediate and final model applications, the representativeness of applied wind field and its spatial variability are not assessed in this study. In spite of these issues and their limitations, the model performance for making plume trajectory estimates was found to be good.

The planning phase model study was important in assessing the probable trajectory of the plume, particularly given the complex flow patterns near Middle Ground. Streamlines based on this initial simulation provided a guide to development of the AUV track. However, results of the preliminary simulation were not favorable when compared with field measurements.

During the intermediate phase of the model effort, it was found that bathymetric variability had a significant effect on the accuracy of Delft3D-FLOW simulations of the near to midfield plume behavior, which is not surprising. Finally, incorporating the effects of stratification was essential in this environment.

Integration with AUV fluorometer data was found to be essential for improving the model. Comparisons of plume delineations derived from the modeling study compare well with those determined from the fluorometer during the active release period. The magnitude of the estimated concentration is systematically lower than measured values. The model was assessed to provide skillful transport estimates focused on active releases and for plume delineation only. Improved model assessments would likely be possible with the benefit of additional release tests.

Care must be taken in order to intercompare HSI and model plume information. Improved light attenuation modeling would improve fidelity of the comparisons between modeled surface plumes and remotely sensed reflectance. This remains an open research question. Significant deviations were found between HSI delineations and either the REMUS fluorometer data and the model estimates.

4.2. Future Research

The value of information feedback between simulations and AUV surveys and HSI products has been demonstrated by this study. Reactive or adaptive AUV survey approaches have been reported by Arrieta et al. [2003] and Farrell et al. [2005]. These approaches could be allied with numerical models as demonstrated within this study. Further, AUVs are available as a platform for a larger suite of water quality measurements [Moline et al., 2005a] and turbulence sensors [MacDonald et al., 2007]. As the number of AUV fielded sensors increase, the opportunities to improve modeling studies also increase and when combined are more useful to a greater variety of research questions.

Acknowledgments

This work was supported by the Office of Naval Research, award N0001406IP20105. We thank the teams at NRL, California Polytechnic State University, and Pacific Northwest National Laboratory for their execution of the field experiment from which this modeling study benefitted greatly. We thank Terri Paluszkiewicz of ONR for guidance and support of this research. We thank all reviewers for their thoughtful comments.

References

Anwar, H. O. (1998), Spread of surface plume in homogeneous and stratified coastal waters, J. Hydraul. Eng., 124(5), 465–473, doi:10.1061/(ASCE)0733-9429(1998)124:5(465).

Arhonditsis, G. B., and M. T. Brett (2004), Evaluation of the current state of mechanistic aquatic biogeochemical modeling, Mar. Ecol. Prog. Ser., 271, 13–26.

Arrieta, R. M., W. Li, J. A. Farrell, and S. Pang (2003), Initial development and testing of an adaptive mission planner for a small unmanned underwater vehicle, in Proceedings of OMAE03, 22nd International Conference on Offshore Mechanics and Arctic Engineering, June 8–13, Cancun, Mexico, pp. 1–9, Am. Soc. of Mech. Eng., New York.

Bielecka, M., and J. Kazmierski (2003), A 3D mathematical model of Vistula Lagoon hydrodynamics: General assumptions and results of preliminary calculations, paper presented at 7th International Conference on Diffuse Pollution and Basin Management, Int. Water Assoc., Dublin.

Brown and Caldwell Consultants (1992), Comprehensive wastewater facilities plan, technical report, Walnut Creek, Calif.

Davis, C. O., M. Kappas, J. Bowles, J. Fisher, J. Antoniades, and M. Carney (1999), Calibration, characterization and first results with the ocean PHILLS hyperspectral imager, in Imaging Spectrometry, edited by M. R. Descour and S. S. Chen, Proc. SPIE Int. Soc. Opt. Eng., 3753, pp. 160–167.

Davis, C. O., et al. (2002), Ocean PHILLS hyperspectral imager: Design, characterization, and calibration, Optics Express, 10, 210–221.

Elwha-Dungeness Planning Unit (2005), Elwha-Dungeness Watershed Plan, Water Resource Inventory Area 18 (WRIA18) and Sequim Bay in West WRIA 17, Entrix, Inc., Concord, Calif.

Farrell, J. A., S. Pang, and W. Li (2005), Chemical plume tracing via an autonomous underwater vehicle, IEEE J. Oceanic Eng., 30(2), 428–442, doi:10.1109/JOE.2004.838066.

Finlayson, D. P. (2005), Combined Bathymetry and Topography of the Puget Lowland, Washington State, http://www.ocean.washington.edu/data/pugetsound/psdem2005.html, School of Oceanogr., Univ. of Wash., Seattle.

Fong, D. A., and N. L. Jones (2006), Evaluation of AUV-based ADCP measurements, Limnol. Oceanogr., 4, 58–67.

Fong, D. A., and M. T. Stacey (2004), Horizontal dispersion of a near-bed coastal plume, J. Fluid Mech., 489, 239–267.

Foreman, M. G. G., R. A. Walters, R. F. Henry, C. P. Keller, and A. G. Dolling (1995), A tidal model for eastern Juan de Fuca Strait and the southern Strait of Georgia, J. Geophys. Res., 100, 721–740.

Grant, S. B., J. H. Kim, B. H. Jones, S. A. Jenkins, J. Wasyl, and C. Cudaback (2005), Surf zone entrainment, along-shore transport, and human health implications of pollution from tidal outlets, J. Geophys. Res., 110, C10025, doi:10.1029/2004JC002401.

Hesselink, A. W., G. S. Stelling, J. C. J. Kwadijk, and H. Middelkoop (2003), Inundation of a Dutch river polder, sensitivity analysis of a physically based inundation model using historic data, Water Resour. Res., 39(9), 1234, doi:10.1029/2002WR001334.

Houghton, R. W. (2002), Diapycnal flow through a tidal front: A dye tracer study on Georges Bank, J. Mar. Syst., 37, 31–46.

Ledwell, J. R., T. F. Duda, M. A. Sundermeyer, and H. E. Seim (2004), Mixing in a coastal environment: 1. A view from dye dispersion, J. Geophys. Res., 109, C10013, doi:10.1029/2003JC002194.

Lin, J., L. J. Pietrafesa, J. S. Ramus, and H. W. Paerl (2007), Water quality gradients across Albemarle-Pamlico estuarine system: Seasonal variations and model applications, J. Coastal Res., 23, 213–229, doi:10.2112/05-0507.1.

Liu, W.-C., J.-T. Kuo, C.-C. Young, and M.-C. Wu (2007), Evaluation of marine outfall with three-dimensional hydrodynamic and water quality modeling, Environ. Model Assess., 12, 201–211, doi:10.1007/s10666-006-9068-0.

MacDonald, D. G., L. Goodman, and R. D. Hetland (2007), Turbulent dissipation in a near-field river plume: A comparison of control volume and microstructure observations with a numerical model, J. Geophys. Res., 112, C07026, doi:10.1029/2006JC004075.

Marmorino, G. O., and G. B. Smith (2007), Infrared imagery of a turbulent intrusion in a stratified environment, Estuaries Coasts, 30, 671–678.

Mofjeld, H. O., and L. H. Larsen (1984), Tides and tidal currents of the inland waters of western Washington, NOAA Techn. Memo. ERL PMEL-56, Pac. Mar. Environ. Lab., Seattle, Wash.

Moline, M. A., P. Bissett, S. Blackwell, J. Mueller, J. Sevadjian, C. Trees, and R. Zaneveld (2005a), An autonomous vehicle approach for quantifying bioluminescense in ports and harbors, in Photonics for Port and Harbor Security, edited by M. J. DeWeert and T. T. Saito, Proc. SPIE Int. Soc. Opt. Eng., 5780, pp. 81–87, doi:10.1107/12.606891.

Moline, M. A., S. M. Blackwell, C. von Alt, B. Allen, T. Austin, N. Forrester, R. Goldsborogh, M. Purcell, and R. Stokey (2005b), Remote Environmental Monitoring UnitS: An autonomous vehicle for characterizing coastal environments, J. Atmos. Oceanic Technol., 22, 1797–1808, doi:10.1175/JTECH1809.1.

Moline, M. A., D. L. Woodruff, and N. R. Evans (2007), Optical delineation of benthic habitat using an autonomous underwater vehicle, Field Robotics, J., 24, 461–471, doi:10.1002/rob.20176.

Pond, S., and G. L. Pickard (1983), Introductory Dynamical Oceanography, 2nd ed., Pergamon, New York.

Ramos, P. A., M. V. Neves, and F. L. Pereira (2006), Mapping and intial dilution estimation of an ocean outfall plume using an autonomous underwater vehicle, Cont. Shelf Res., 27, 465–473, doi:10.1016/j.csr.2006.11.017.

Stacey, M. T., E. A. Cowen, T. M. Powell, E. Dobbins, S. G. Monismith, and J. R. Koseff (2000), Plume dispersion in a stratified, near-coastal flow: Measurements and modeling, Cont. Shelf Res., 20, 637–663.

WL Delft Hydraulics (2003), Deflt3D-FLOW: Simulation of Multi-dimensional Hydrodynamic Flows and Transport Phenomena, Including Sediments, User Manual, Delft, Netherlands.

Figures

Figure 1

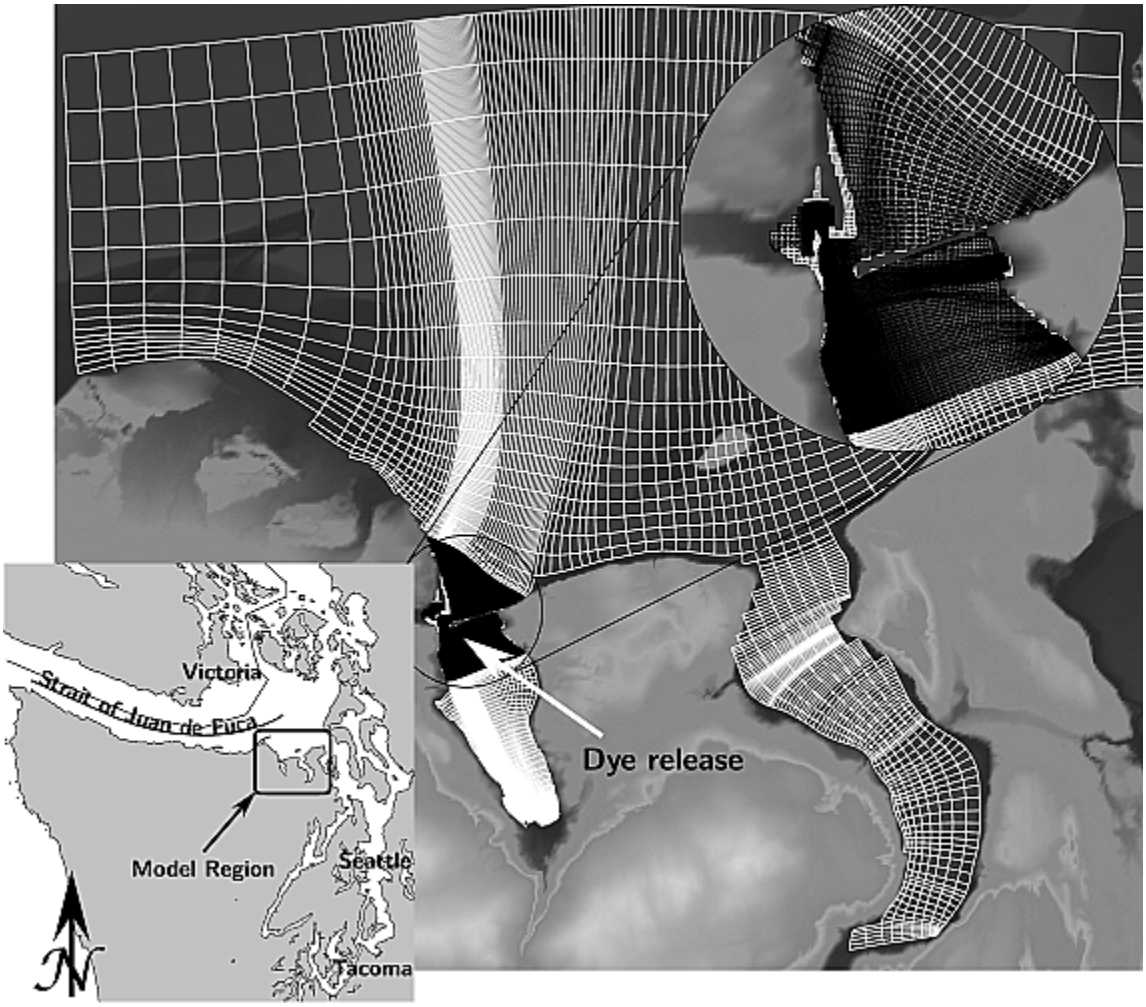

Figure 1. Model meshes used. Nested mesh is shown in black, surrounding the dye release point. The inset is a regional map showing the geographic area.

Figure 2

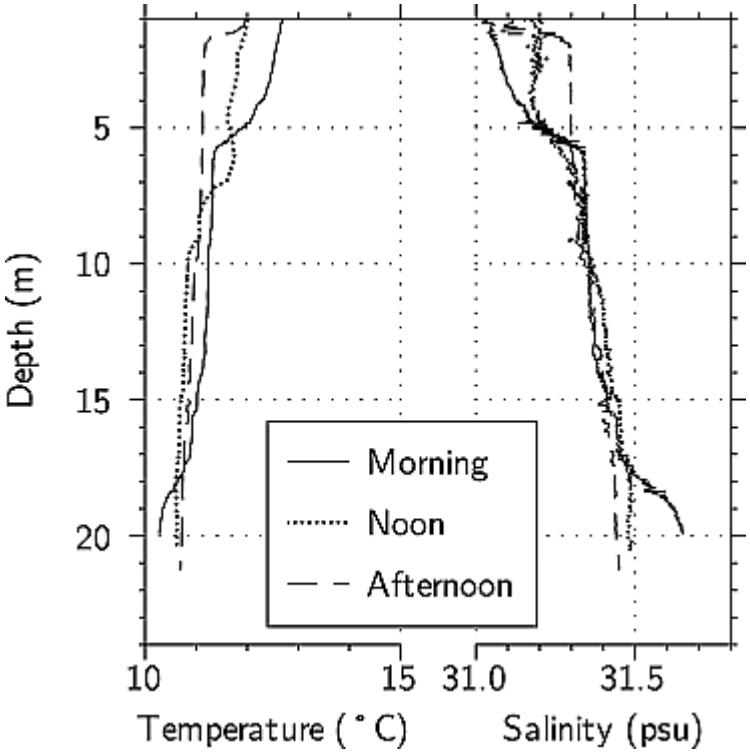

Figure 2. CTD profiles for incoming (morning), slack (noon), and incoming (afternoon) of 20 July. The height of the upper layer appears to vary by approximately 5 m.

Figure 3

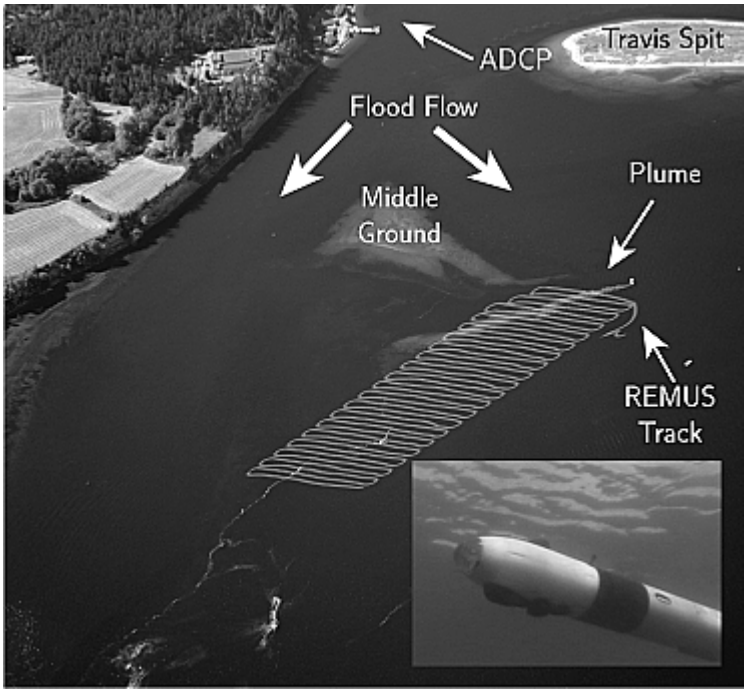

Figure 3. Aerial photograph of dye plume in Sequim Bay, near the end of the active release period. Geographic features are labeled for reference; plume travel direction is approximately right to left in this photo.

Figure 4

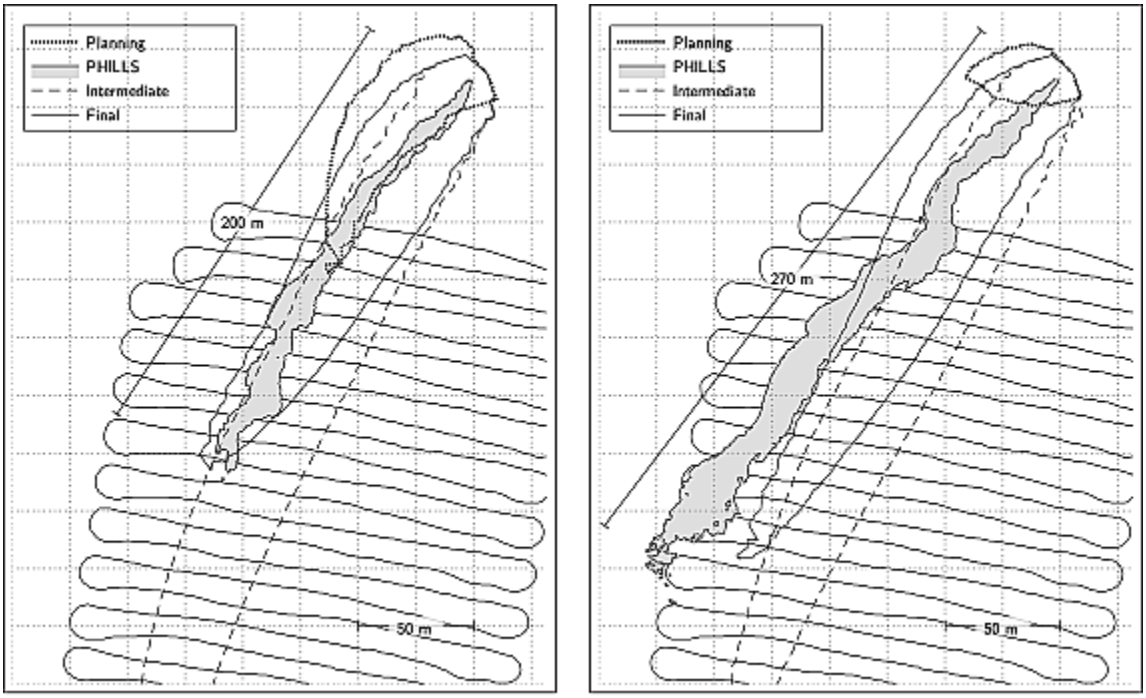

(a) Comparison of HSI and model concentrations at 1625.

(b) Comparison of HSI and model concentrations at 1649.

Figure 4. Comparison of model results for various configurations compared with HSI normalized signals at two time instances. Model results were normalized by the highest predicted concentration at each time.

Figure 5

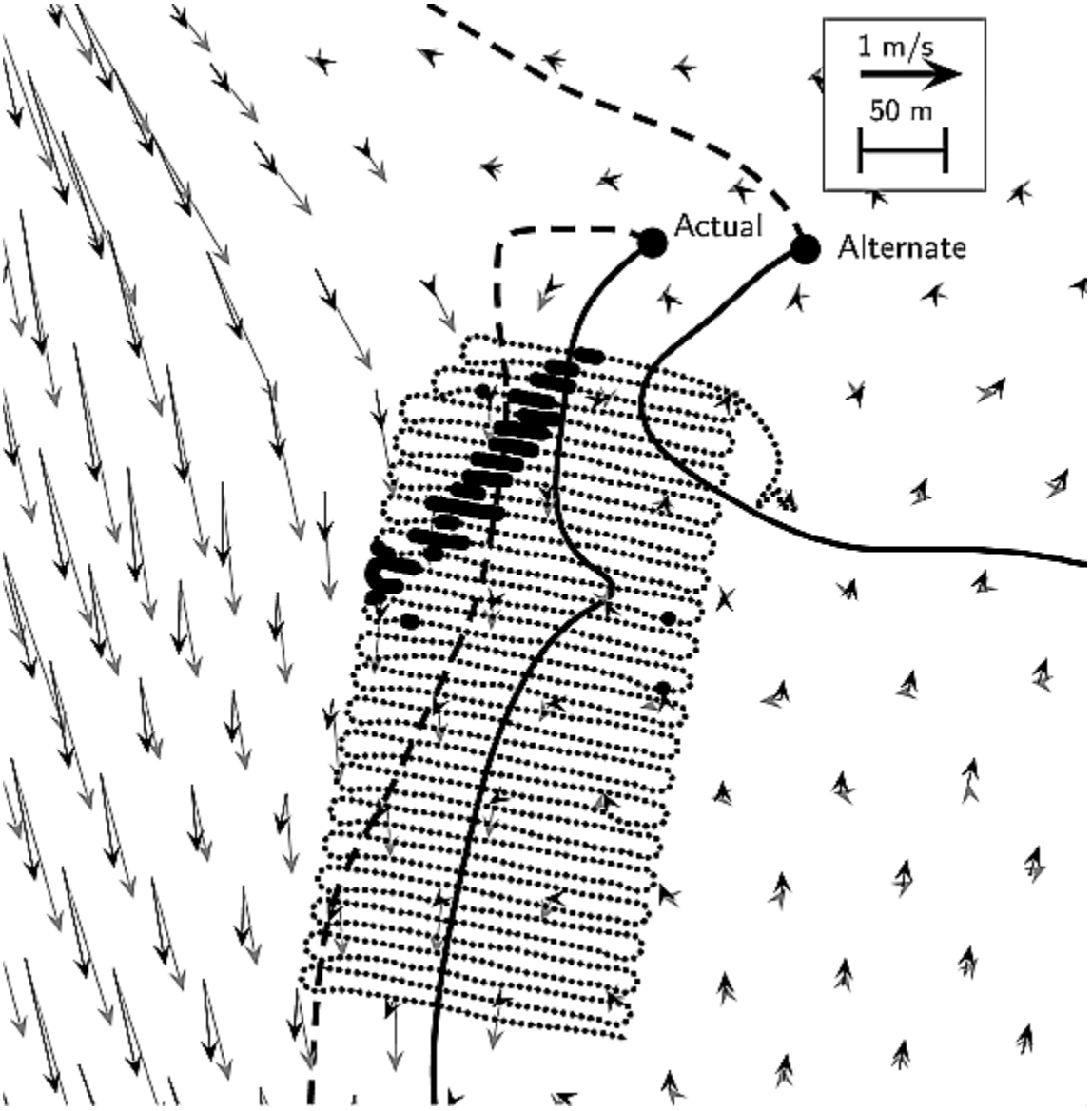

Figure 5. Planning model circulation results showing flow patterns near the plume release for the actual release location and an alternate location. The solid streamlines and light colored vectors correspond to the RWT release start time, and the dashed streamlines and dark colored vectors correspond to the RWT release stop time. The estimated release location and streamlines were used to orient the AUV track shown as a fine dotted line. Larger dots on the track indicate where the fluorometer detected RWT after execution of the planning phase of the modeling effort.

Figure 6

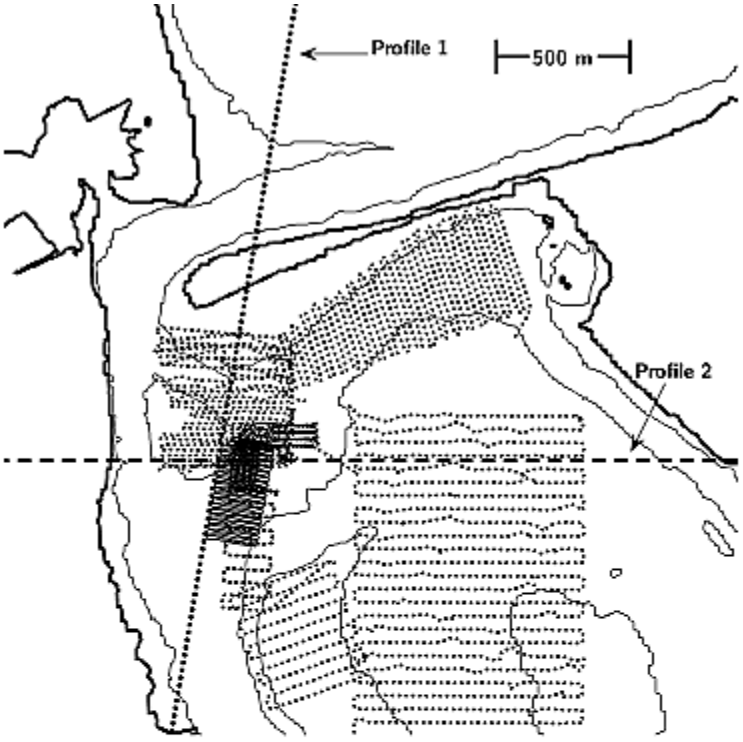

(a) Bathymetry surveys were conducted in the dotted line areas. The solid (dark) line indicates the plume survey.

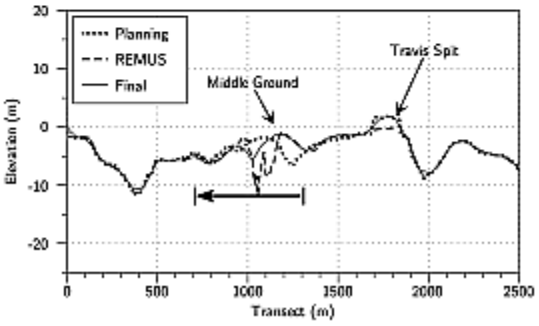

(b) Profile #1, taken parallel to the plume body. Arrow denotes approximate extent and direction of plume.

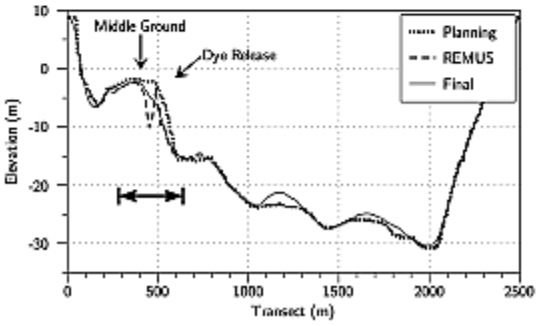

(c) Profile #2, taken East-West across the plume body. Arrow denotes approximate area of survey/dye release.

Figure 6. Bathymetry of Sequim Bay in the plume experiment region. Depths are in meters relative to mean lower low water, and vertical scale of the line graphs (Figures 6b and 6c) is significantly distorted.

Figure 7

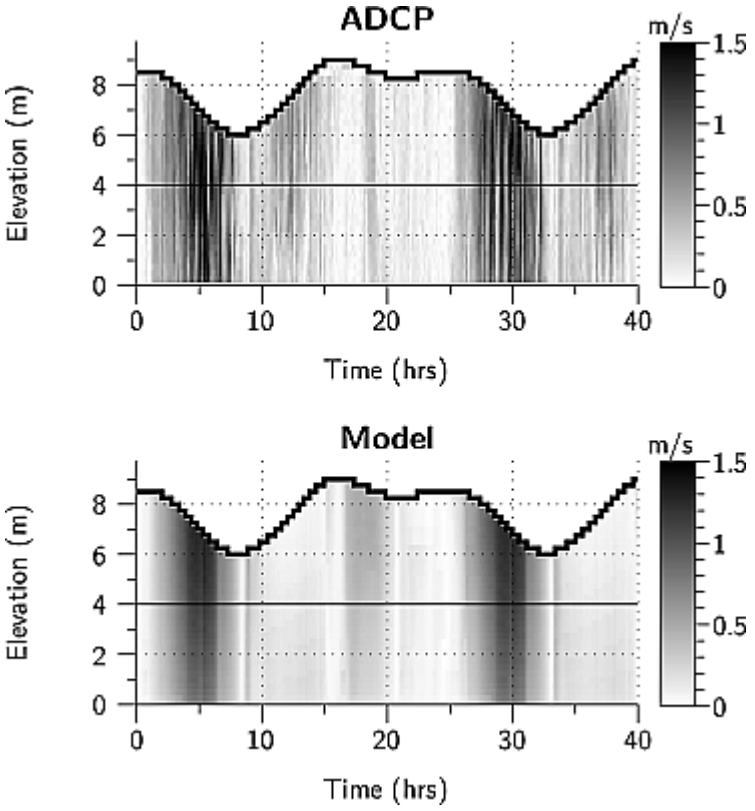

Figure 7. (top) ADCP and (bottom) model current magnitude profiles (m/s). Dye release occurred on incoming tide at ~15 h. Figure 8 shows sections of current speed at the 4 m level, denoted here by a black line.

Figure 8

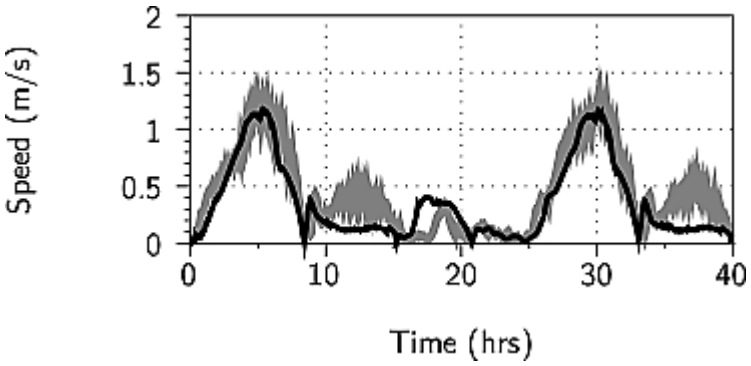

Figure 8. Time series of ADCP (gray line) and model (black line) current speed at the 4 m level noted in Figure 7. Box smoothing with a window of 4 min was applied to the ADCP data.

Figure 9

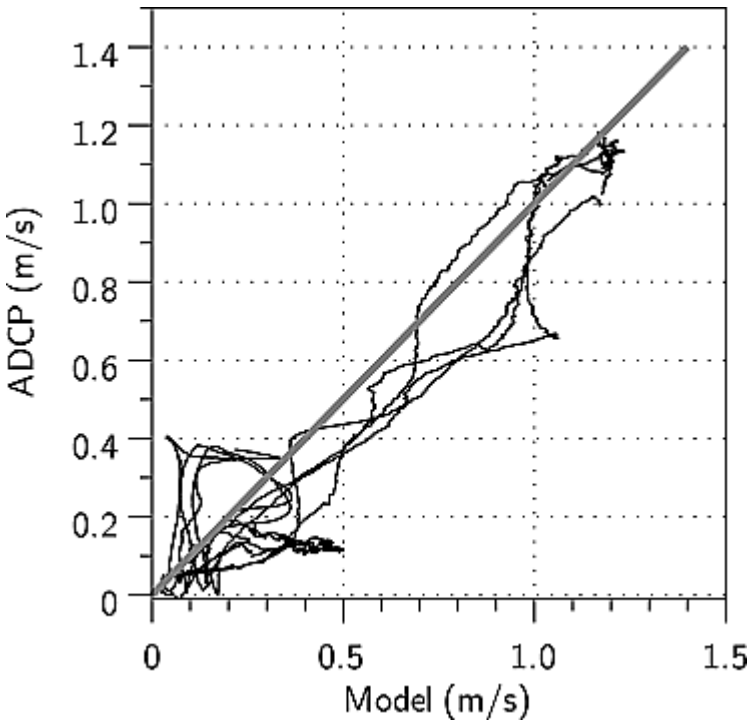

Figure 9. Smoothed ADCP values using a box filter with a window of 4 min versus predicted current speed at the 4 m elevation (see Figure 7).

Figure 10

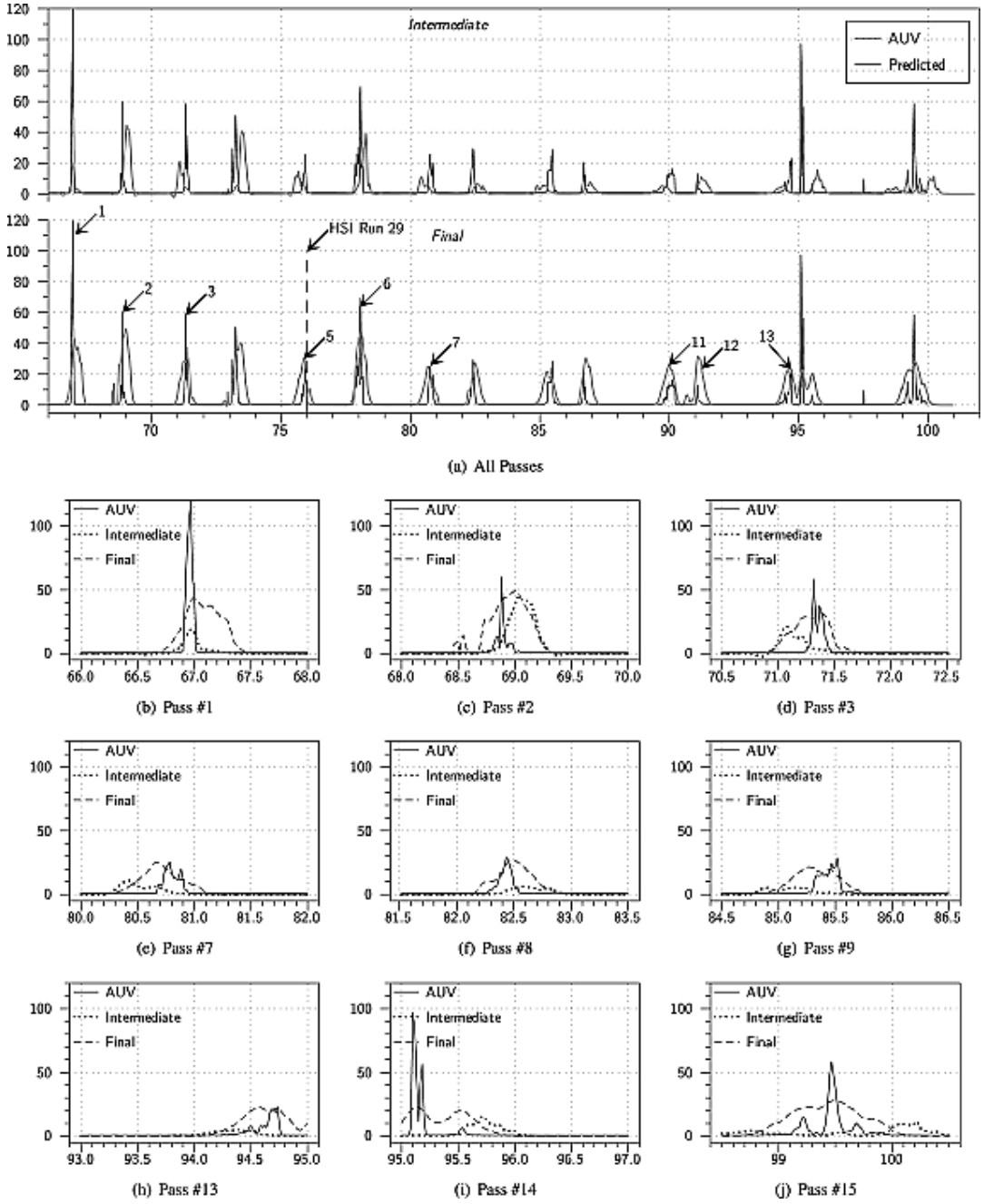

Figure 10. Comparison of model results for intermediate (unstratified) and final (stratified) simulations with measured transects. Vertical axis is concentration in ppb, and horizontal axis is elapsed time in minutes since the simulation began.

Figure 11

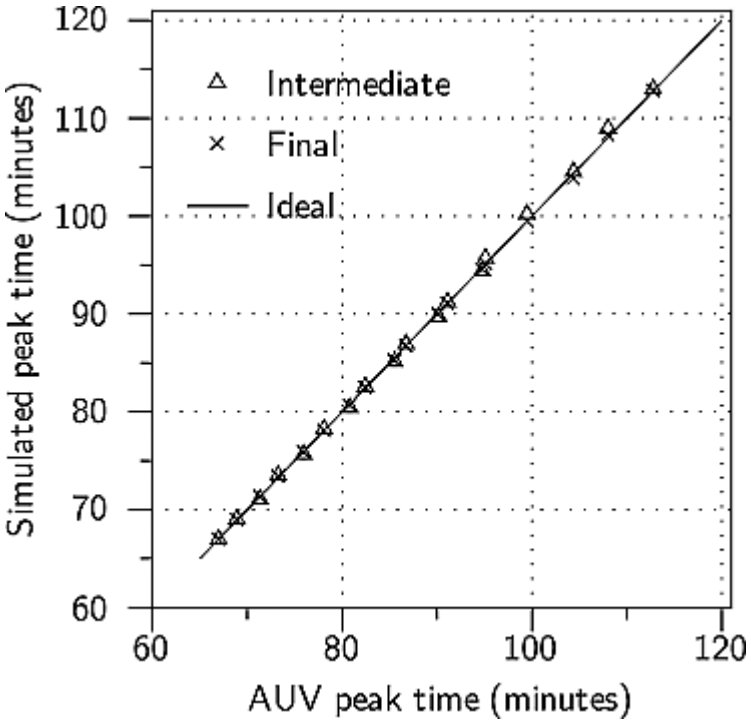

Figure 11. Comparison of elapsed time at peak concentration for Delft3D and the AUV for the final and intermediate simulations. The 45° line indicates a perfect fit.

Tables

Table 1: Model Phases

Final		Planning	Intermediate
Bathymetry Source	Finlayson [2005]	Finlayson [2005] & REMUS survey	Finlayson [2005] & REMUS
Sidewall Boundary	free-slip	free-slip	no-slip
Stratification	none	none	24 July, CTD cast
Wind forcing	none	Measured	measured
Tidal Forcing	Flatera	Flatera	Flatera
Wind Waves	none	none	none

aD. Flater (http://www.flaterco.com/xtide, 2006).

Table 2: Nested Model Characteristics

	Coarse Mesh	Fine Mesh
Mesh size	108 × 132	187 × 145
Mesh extent (km)	33 × 28	2.6 × 3.4
Nominal horizontal resolution (m)	250	20
Number of vertical layers	10	10
Time step (min)	1	1
Archive interval (min)	5	N/A
Starting time (PDT)	22 July 2007 1800	24 July 2007 1200
Ending time (PDT)	26 July 2007 1800	24 July 2007 1800
Horizontal eddy diffusivity (m^2/s)	10	0.02–0.1
Horizontal eddy viscosity (m^2/s)	1	1

Table 3: Layer Δσ Thicknesses Used in Each Model Application

Layer	Coarse	Fine
1	20	4
2	20	6
3	15	8
4	12	10
5	10	15
6	8	15
7	6	15
8	4	12
9	3	9
10	2	6
Total	100	100

Table 4: The 24 July 2007 HSI Collection Clock Time, Time Relative to RWT Release Start and Time Relative to AUV Survey Initiation[a]

Run	Time (PST)	$Time_{dye}$[b] (min)	$Time_{AUV}$[c] (min)	Geographic Adjustment (m) (Easting,Northing)	Band Ratio Maxima	Comment
14	16:00	27	30	0, 0	46.2	geographic baseline
22	16:25	52	55	10, -1	49	active RWT release
29	16:49	76	79	4, -11	46.3	spectral baseline
37	17:15	-25	105	17, -17	34.1	post-RWT release
41	17:29	-39	119	2.5, -1	7	23.3 post-RWT release
44	17:46	-54	136	16, -30	21.6	post-RWT release

[a]Collection times after RWT ceased are shown parenthetically. Geographic adjustment expressed in meters. HSI 592.2/533.6 band ratio maxima for each image is included.

[b]Time relative to start or end of dye release (relative to end in parentheses).

[c]Time relative to AUV mission start